PHYSICAL REVIEW B **81**, 125328 (2010)

Charge-optimized many-body potential for the hafnium/hafnium oxide system

Tzu-Ray Shan (單子睿), Bryce D. Devine, Travis W. Kemper, Susan B. Sinnott, and Simon R. Phillpot*

Department of Materials Science and Engineering, University of Florida, Gainesville, Florida 32611-6400, USA

(Received 9 December 2009; revised manuscript received 26 February 2010; published 24 March 2010)

A dynamic-charge, many-body potential function is proposed for the hafnium/hafnium oxide system. It is based on an extended Tersoff potential for semiconductors and the charge-optimized many-body potential for silicon oxide. The materials fidelity of the proposed formalism is demonstrated for both hafnium metal and various hafnia polymorphs. In particular, the correct orders of the experimentally observed polymorphs of both the metal and the oxide are obtained. Satisfactory agreement is found for the structural and mechanical properties, defect energetics, and phase stability as compared to first-principles calculations and/or experimental values. The potential can be used in conjunction with the previously determined potentials for the Si and SiO_2 system. This transferability is demonstrated by comparing the structure of a hafnia/silicon interface to that previously determined from electronic-structure calculations.

DOI: 10.1103/PhysRevB.81.125328 PACS number(s): 31.15.−p, 34.20.Cf, 77.55.df

I. INTRODUCTION

The continuous downsizing in the feature dimensions of microelectronic devices and ultralarge integrated circuits (ULSIs) dimensions has necessitated ever thinner dielectric oxide layers. Silicon dioxide (SiO_2, silica) had been used as the gate oxide for decades. However it had to become so thin (~1 nm) that the generation of leakage current had become a serious problem. To overcome this limitation, oxide materials with higher dielectric constants are replacing silica. Of all the oxide materials explored to date, hafnium dioxide (HfO_2, hafnia) is considered to be one of the most important because of its relatively high dielectric constants (typically 20–25 depending on the polymorphs),[1,2] and high thermal stability when in contact with silicon (both semiconductor and poly-Si gate electrode).[3] Moreover, it has been reported both experimentally and computationally that the incorporation of nitrogen[4,5] and fluorine[6,7] into hafnia films used in current devices further reduces the leakage current by passivating the oxygen vacancies.[8] However challenges still remain. In particular, the formation of a low dielectric-constant hafnium silicate interfacial layer[9] and the presence of oxygen defects at both the hafnia/silicon interface and in the hafnia film that trap electrons lead to a decrease in channel mobility and an instability in the threshold voltage.[10,11]

Hafnia crystallizes into three crystalline polymorphs at ambient pressure: a monoclinic ($P2_1/c$) phase, a tetragonal ($P4_2nmc$) phase, and a cubic fluorite ($Fm\bar{3}m$) phase. The monoclinic-to-tetragonal transition takes place at 2000 K while the tetragonal-to-cubic transition occurs at 2900 K. The melting point of the cubic phase is at 3085 K.[12] There are also two high-pressure phases: the orthorhombic I phase (*Pbca*, Brookite-type structure) above 10 GPa and the orthorhombic II phase (*Pnma*, $PbCl_2$-type, or cotunnite structure) above 30 GPa.[13] Monoclinic hafnia has a band gap of 5.68 eV.[14]

Computational studies on hafnia and on the critical HfO_2/Si interfaces rely heavily on *ab initio* quantum-mechanical[15] and density-functional theory (DFT) methods.[16,17] Although electronic-structure methods provide the highest accuracy currently available, they are computer-time intensive and limited to systems sizes of typically a few hundred atoms. Because of these size limitations and the difficulty in simulation at nonzero temperatures, electronic-structure methods are not well suited to the investigation of certain phenomena that are of interest, such as the evolution of device-size HfO_2/Si interfaces, the growth of hafnia films on Si surfaces with pulsed laser deposition (PLD), ion diffusion, and thermal transport. The strengths and weaknesses of classical molecular-dynamics (MD) simulations are complementary to those of first-principles calculations: the empirical interatomic potentials do not promise the level of materials fidelity of electronic-structure methods; however, they can simulate large systems and capture nonzero temperature and dynamical processes in a natural way. Currently, no published empirical potential predicts monoclinic hafnia to be the most stable phase or correctly describes the properties of hafnia polymorphs. A charge-optimized many-body (COMB) potential, which allows dynamic charge equilibration, has previously been developed for Si/SiO_2 systems.[18] It has recently been improved and extended to include amorphous silica[19] and well describes the properties and phase order among silicon and silica polymorphs. In this paper, therefore, we develop a COMB potential that, by design, gives the correct phase order and reasonably well reproduces key properties of both elemental hafnium and hafnia polymorphs. Moreover, the potential is compatible with the previously developed potentials for the Si/SiO_2 system and amorphous silica,[19] allowing the simulation of HfO_2/Si interfaces.

The rest of the paper is organized as follows. In Sec. II we introduce the general COMB potential formalism for Hf/HfO_2 and compare the predicted properties of hafnium metal and hafnia polymorphs to experimental values. In Sec. III we evaluate the point-defect energetics for this the potential while in Sec. IV we apply the potential to study the interfacial structure, work of adhesion, and charge transfer of an HfO_2/Si interface. Section V contains a discussion and our conclusions.

II. COMB POTENTIAL FOR THE HAFNIUM/HAFNIUM OXIDE SYSTEM

The COMB potential for Hf/HfO_2 is built on the physical and mathematical framework developed for the Si/SiO_2 sys-

 ©2010 The American Physical Society

tem, described more fully elsewhere.[19,20] Briefly, the COMB potential formalism is based on the empirical Tersoff potential for silicon.[21,22] The Tersoff potential describes many-body interactions, allows the breaking of existing bonds and the formation of new bonds, and has been successfully applied to study various properties of silicon and diamond. Building on the Tersoff potential, Yasukawa[23] extended the bond-order method to the Si/SiO_2 system by adding an electrostatic term and self-consistent charge equilibration in the spirit of the Rappe and Goddard approach,[24] which was also applied to Al/Al_2O_3 by Streitz and Mintmire[25] and most recently by Devine *et al.*[20] to Cu/Cu_2O. Iwasaki *et al.*[26,27] applied the same Yasukawa approach to the Si/HfO_2, Ge/HfO_2, and Si/ZrO_2 systems, while Yu *et al.*[18] modified the Yasukawa potential function by adding bond-bending terms for Si-O-Si and O-Si-O, yielding the COMB framework for the modified form for Si/SiO_2 and amorphous silica.[19] COMB was able to capture the correct phase stability of the SiO_2 polymorphs.

Although these extended-Tersoff potentials have their strengths, including the ability to model multicomponent heterogeneous systems and transferability among different species, they are limited because of the use of a damped point-charge model and because of the unrealistically short cutoff for the electrostatic term in the potential. To rectify these deficiencies, Devine *et al.*[20] modified the extended Tersoff potential for the Cu/Cu_2O systems (COMB potential for Cu/Cu_2O) by replacing the point-charge model and the cutoff function with Coulomb integrals over Slater 1*s* orbital[28] and by treating the electrostatic interactions using the real-space direct summation of modules.[29] In this paper these improvements to the COMB formalism are incorporated into the formalism for the Hf/HfO_2 systems.

A. General formalism

The COMB potential for Hf/HfO_2 system has the same general form as that for the Si/SiO_2 systems[19] and Cu/Cu_2O systems.[20] The reader is referred to Appendix and Refs. 19 and 20 for full details of the general functional formalism. Here, only terms specific to the Hf/HfO_2 system are discussed.

The bond-bending term E_i^{BB} used here is different from the COMB potential for Cu/Cu_2O, which uses a third-order Legendre polynomial[30] defined as

$$E^{BB}_{\text{Cu-Cu-Cu}} = \sum_i \sum_{j\neq i} \sum_{k\neq i,j} f_{S_{ij}} f_{S_{ik}} [K^3_{LP} P^3(\cos\,\theta_{\text{Cu-Cu-Cu}})], \quad (1)$$

where P^3 is the third-order Legendre polynomial function of the Cu-Cu-Cu bond angle and K^3_{LP} is the coefficient fitted to the difference in cohesive energies of Cu in hexagonal-close-packed (hcp) and face-centered-cubic (fcc) phases. This function penalizes the 109.47° angle of the hcp phase in order to make the fcc phase more stable. When applying this function to Hf, however, the leading coefficient K^3_{LP} must be negative since hcp is the more stable phase. Also, the absolute value of the fcc-hcp energy difference for Hf is approximately an order of magnitude greater than that of Cu; thus K^3_{LP} must be a larger negative number. Although this function with a negative leading coefficient does successfully stabilize the 109.47° bond angle of the hcp phase, it also penalizes the 146° angle that is specific to the hcp phase. This penalty is significant because of the large K^3_{LP} value and results in an unstable hcp phase above 200 K.

To overcome this problem while still retaining a more stable hcp phase, this work instead employs a sixth-order Legendre polynomial as the bond-bending term E_i^{BB} applied only to Hf-Hf-Hf bonds. The function is defined as

$$E^{BB}_{\text{Hf-Hf-Hf}} = \sum_i \sum_{j\neq i} \sum_{k\neq i,j} f_{S_{ij}} f_{S_{ik}} [K^6_{LP} P^6(\cos\,\theta_{\text{Hf-Hf-Hf}})], \quad (2)$$

where P^6 is the sixth-order Legendre polynomial function of the Hf-Hf-Hf bond angle and K^6_{LP} is the coefficient fitted to the difference in cohesive energies of Hf in hcp and fcc phases. This function stabilizes the 146° Hf-Hf-Hf bond angle of the hcp phase, without significantly penalizing the 109.47° angle. With this polynomial function, the hcp phase of Hf is stable and the hcp-fcc energy difference is well described.

When applying the COMB potential to model pure Hf metal, the charge-dependent terms do not contribute to the energy; as a result the potential formalism is significantly simplified. This reduced form of the potential has been previously been applied to fcc Cu by Yu *et al.*,[31] and full details can be found in Ref. 31.

The challenge for the hafnia system is the variety of Hf-O-Hf and O-Hf-O bond angles that are displayed by the various hafnia phases. For this reason, attempts to stabilize the monoclinic phase with bond-bending terms applied to Hf-O-Hf and O-Hf-O at first proved unsuccessful. Therefore, we introduce an overcoordination correction term to destabilize the phases with higher (8 and greater) coordination number on the Hf atom. This term was inspired by the analogous term in the ReaxFF potential for hydrocarbons[32] and takes the form for the Hf-O system,

$$E_{over} = f_c E_0 \Delta N^* \left[\frac{1}{1+\exp(\gamma \Delta N)}\right], \quad (3)$$

$$\Delta N = \sum f_c(r_{\text{Hf-O}}, R_S, S_S). \quad (4)$$

Here E_0 and γ are fitted parameters that control the strength of the overcoordination correction, and ΔN is the overcoordination number with respect to 7 (the coordination number of Hf atom in the ground-state monoclinic phase). The calculation of ΔN incorporates the short-range cutoff f_c, defined here in Eq. (A24), where R_S and S_S are the inner and outer covalent cutoffs, respectively, and are defined in Table I. This correction term is only applied when ΔN is greater than 0.25.

Upon annealing, however, the tetragonal phase transformed into the cubic phase, whereas the transition identified by the c/a ratio being close to 1.0 and very similar Hf-O bond lengths (close to 2.19 Å) around any particular Hf atom (instead of four shorter bonds at 2.08 Å and four longer ones at 2.39 Å as in the tetragonal phase). Therefore, we introduce an additional repulsion term that takes the form,

TABLE I. Potential parameters for Hf and O for the COMB potential for Hf/HfO_2 developed in this work.

	Hf	O
A (eV)	707.5303	3326.699
B (eV)	55.94216	260.8931
λ (Å^{-1})	2.069563	5.36
α (Å^{-1})	0.959614	2.68
β	0.046511	2.0
n	1.011011	1
m	1	1
c	0	6.6
d	1	1
h	0	−0.229
R_S	3.40	2.6
S_S	4.20	3.0
Q_L	−4.0	−1.8349
Q_U	4.0	5.5046
D_L	0.26152	0.00148
D_U	−0.25918	−0.00112
n_B	10	10
C_{VDW}	0	0
X	0	5.63441
J	3.13952	7.68960
K	0	4.51427
L	0.00941	1.33008
ξ	0.679131	2.243072
ρ_1	−3.928750	−3.922011
ρ_2	4.839580	0.971086
K_{LP}^6	0.008	
R_Ω	0.14	
E_0	0.16	
γ	0.10	

$$E_r = f_{c_1} f_{c_2} R_\Omega (50x^4 - 30x^2 + 4.5)/8, \tag{5}$$

where

$$x = (r_1 - r_{\text{Hf-O}})/(r_1 - r_2). \tag{6}$$

The leading coefficient R_Ω is 0.14 eV, r_1 and r_2 are 2.2285 Å and 1.8935 Å, respectively, and $r_{\text{Hf-O}}$ is the Hf-O bond length. These additional terms, E_{over} and E_r, are added into the repulsive energy term, Eq. (A3).

B. Fitting procedure

We have developed an algorithm that fits structural and energetic information for multiple phases. It determines the potential parameter set using a least-squares method to minimize a penalty function, $f(p)$, for each trial parameter set, p. The penalty function is determined for all included phases by calculating the variation in lattice parameters, elastic constants, and energy as a function of isometric strain with respective to the target values (obtained from first-principles calculations or experiments) with corresponding fitting weights. We have included a total of eight phases in the fitting procedure for the COMB potential for Hf/HfO_2: the ambient-pressure monoclinic, tetragonal, and cubic phases, high-pressure orthorhombic I (OI) and orthorhombic II (OII) phases, rutile ($P4_2/mnm$) and α-PbO_2 ($Pbcn$) phases, and the pure Hf hexagonal metal phase ($P6_3/mmc$). The Hf metal in fcc phase was not included in the fit because the fcc-hcp energy difference is solely dependent upon the Legendre polynomial and can be incorporated after all the other parameters have been fitted. The rutile and α-PbO_2 type phases do not appear in the phase diagram of hafnia, but some empirical potentials for AX_2 system have predicted them to be low-energy states, or even the ground state. This has been an endemic problem in developing potentials for monoclinic zirconia, ZrO_2.[33–35] Hence, we include these two phases in the fit to ensure that they are much higher in energy than the experimentally observed phases.

Since the parameterization of the Iwasaki potential for Si/HfO_2 was determined by fitting the atomic forces obtained with the potential to those obtained from first-principles calculations on Ge/ZrO_2 or Si/HfO_2 interfacial models, the potentials did not necessarily reproduce the structural and mechanical properties of the hafnium metal and hafnium oxide polymorphs, as discussed in more detail below. However, the parameter set from the Iwasaki potential is still a valuable guideline and is used as the initial guess in our fitting procedure. The final parameterization for the Hf/HfO_2 COMB potential is shown in Table I.

C. Properties of Hf metal predicted by the COMB potential

Table II compares the properties of hafnium metal predicted by the COMB potential with values from experiments, first-principles calculations, and the Iwasaki potential. Since Iwasaki did not publish these values in Refs. 26 and 27, we implemented his potential in our in-house MD code and calculated the properties with the published parameters.

It can be seen from Table II that the COMB potential not only predicts the lattice constants of Hf better than the Iwasaki potential but also yields almost exact agreement with experimental values for the elastic constants and the bulk and shear moduli. Most importantly, the COMB potential gives the correct order among different phases. In particular for metallic Hf, the energy difference between the hcp and fcc phases is very close to that calculated from DFT calculations. This is actually straightforward to achieve with the COMB potential since fcc and hcp phases cannot be distinguished with first-nearest-neighbor potentials without additional correction terms. Fitting the K_{LP}^6 coefficient for the Legendre polynomial of the COMB potential gives the right hcp-to-fcc phase order with the exact energy difference. The Iwasaki potential does not contain a correction term such as that used here, and hence predicts zero-energy difference between the fcc and hcp phases.

With an almost exact fit to the hcp-to-fcc energy difference, the COMB potential also predicts the unstable stacking fault energy as 1.695 J/m^2, which is very close to the value

TABLE II. Properties of hafnium metal given by the COMB potential for Hf/HfO_2 developed in this work in comparison with experimental, DFT calculations, and the Iwasaki potential.

Properties	Expt.	COMB	DFT (PBE)	Iwasaki
a_0 [a] (Å)	3.1950	3.167	3.1935	3.1389
c_0 [a] (Å)	5.0542	5.147	5.0533	5.1276
E_c [a] (eV/atom)	−6.99	−6.98	−9.96	−6.59
C_{11} [a] (GPa)	190	195		201
C_{12} [a] (GPa)	75	75		69
C_{13} [a] (GPa)	66	65		63
C_{33} [a] (GPa)	204	209		220
C_{44} [a] (GPa)	60	53		58
C_{66} [a] (GPa)	58	61		66
B [a] (GPa)	110	112	114.59	112
G [a] (GPa)	61	60		65.1
E (fcc-hcp)[a] (eV/atom)		0.055	0.060	0.0
E (bcc-hcp) (eV/atom)		0.188	0.155	2.273
E (dia-hcp) (eV/atom)		3.98	2.07	3.768
Unstable stacking fault (J/m^2)		1.695	1.662	
$\gamma(0001)$ (mJ/m^2)		2250	1133	3006
$\gamma(1\bar{1}00)$(mJ/m^2)		2466	2003	4002
$\gamma(2\bar{1}\bar{1}0)$(mJ/m^2)		2936	3044	3752
Vacancy (eV/defect)		4.62	2.55	
Interstitial (eV/defect)		6.17	6.23	
α (10^{-6} K^{-1})	5.9	6.9		

[a]Denotes fitted properties.

of 1.662 J/m^2 calculated from DFT. Also shown in Table II are linear thermal expansion coefficients, 6.9×10^{-6} K^{-1} and 5.9×10^{-6} K^{-1}, predicted from the COMB potential and from experiments, respectively, and the defect-formation energies of Hf vacancy and interstitial. The COMB potential predicts the right trend and an interstitial formation energy very close to the DFT value; however, the COMB potential predicts a vacancy formation energy in Hf metal that is larger than that from DFT calculation by almost a factor of 2. This is also the case for the surface energies, COMB predicts the right trend for the surface energies but the values are approximately twice as large as the values from the DFT calculations for some of the surfaces considered. These overestimations are consistent with the overestimation of the bulk cohesive energy.

D. Properties of HfO_2 phases and phase stability from the COMB potential

Table III compares of the properties of the monoclinic, tetragonal, and cubic hafnia phases predicted by the COMB potential with experiment, DFT calculations, and the Iwasaki potential. The properties from the Iwasaki potential were again calculated with our implementation of the potential. Using a damped force minimization (quench) method with the Iwasaki potential, the monoclinic phase spontaneously transforms to a phase that resembles the α-PbO_2-type structure with a much lower cohesive energy than the monoclinic phase. As a result, the properties for the monoclinic phase predicted from the Iwasaki potential are left blank in Table III. The Iwasaki potential predicts higher cohesive energies for the monoclinic and tetragonal phases than for the α-PbO_2-type structure; thus these phases are metastable in the Iwasaki potential. Not shown in the table are the relaxed surface energies for the (111), (001), and (100) surfaces of the monoclinic phase: 1.07 J/m^2, 1.17 J/m^2, and 2.02 J/m^2, respectively, compared to 1.25, 1.45, and 1.79 J/m^2 from a first-principles study.[44]

By construction, the COMB potential reproduces the phase order and elastic properties of the hafnia phases reasonably well. The monoclinic phase is the most stable structure with the COMB potential, which is in agreement with both experiments and DFT calculations. This is demonstrated in Fig. 1(a), which illustrates the cohesive energies as a function of unit volume (E-V curves) for various hafnia phases calculated from DFT with Perdew-Burke-Ernzerhof (DFT-PBE) exchange-correlation functional,[45] and Fig. 1(b), which shows the corresponding data for the COMB potential. As is the case in the DFT calculations, the high-pressure OI phase has a lower energy than the tetragonal phase, and the equilibrium volume is substantially smaller than that of the monoclinic and tetragonal phases. The transition barrier should be high enough to prevent the undesired monoclinic-to-OI phase transition.

Table IV quantifies this comparison, showing the cohesive energies of monoclinic, tetragonal, cubic, OI, and OII hafnia

TABLE III. Fitted properties of monoclinic, tetragonal, and cubic hafnia phases given by the COMB potential for Hf/HfO_2 developed in this work in comparison with that from experiments, first-principles calculations, a Buckingham-type potential, and the Iwasaki potential.

Properties	Expt.	COMB	DFT	Iwasaki[a]
Monoclinic HfO_2				
a_0 (Å)	5.12[b]	5.13	5.12[c,d]	
b_0 (Å)	5.17[b]	5.21	5.20[c,d]	
c_0 (Å)	5.30[b]	5.11	5.28[c,d]	
β (deg)	99.2[b]	98.8	99.7[c,d]	
E_c (eV/HfO_2)		−30.89	−30.56	
B (GPa)		235	251[e]	
G (GPa)		120		
$q_{Hf}(e)$		3.48	3.60[d]	3.38
Tetragonal HfO_2				
a_0 (Å)	5.151[b]	5.03	5.059[d]	4.921
c_0 (Å)	5.29[b]	5.05	5.1996[d]	6.26
E_c (eV/HfO_2)		−30.79	−30.40	−41.85
B (GPa)	210[f]–281[g]	307	197[d]–240	585
G (GPa)		154	128	342
C_{11} (GPa)		567	495	1151
C_{12} (GPa)		179	152	302
C_{13} (GPa)		176	115	302
C_{33} (GPa)		564	397	1149
C_{44} (GPa)		126	90	288
C_{66} (GPa)		128	125	288
$q_{Hf}(e)$		3.46	3.33[d]	3.30
Cubic HfO_2				
a_0 (Å)	5.08[b]	5.02	5.05[c]	6.25
E_c (eV/HfO_2)		−30.76	−30.32	−40.74
B (GPa)		295	201[d]–280[e]	556
G (GPa)		200	229[h]	324
C_{11} (GPa)		561	578[h]	1098
C_{12} (GPa)		161	121[h]	285
C_{44} (GPa)		111	83[h]	270
$q_{Hf}(e)$		3.44	3.49[d]	3.22

[a]Properties for the monoclinic phase are left blank, see text for explanation.
[b]References 36–38.
[c]Reference 39.
[d]Reference 40.
[e]Reference 41.
[f]Reference 13.
[g]Reference 42.
[h]Reference 43.

phases calculated from DFT-PBE and the COMB potential relative to the monoclinic phase. The DFT calculations of these known phases from this work are in excellent agreement with the literature[40] and the correct phase order of the phases is captured by the COMB potential. Also given in the table are the cohesive energies of the rutile and α-PbO_2-type phases; it can be seen that the α-PbO_2-type HfO_2 structure is predicted by the DFT calculations to have the second lowest energy even though it does not exist in nature. The reason for the absence of α-PbO_2-type phase in experiment may be attributed to the fact that large negative pressure is required for a monoclinic phase to transform to an α-PbO_2 type, as indicated by the larger equilibrium volume of the α-PbO_2 system illustrated in Fig. 1(a). The fact that this phase is predicted to be so low in energy could also be a shortcoming of the DFT-PBE calculations. Although the order of the rutile and α-PbO_2-type HfO_2 structures predicted from the COMB potential is opposite to that from the DFT-PBE calculations, in

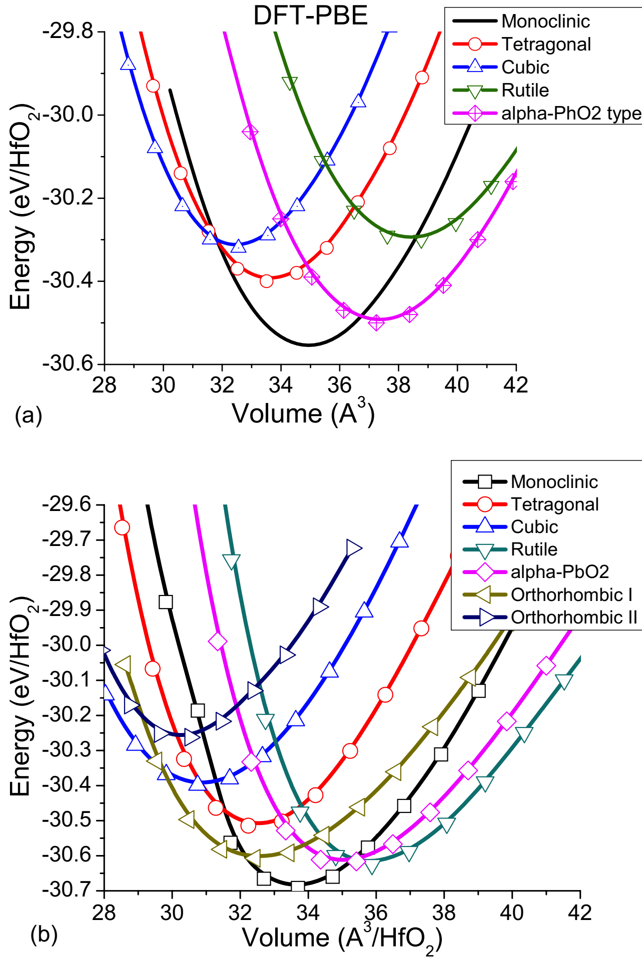

FIG. 1. (Color online) Cohesive energies as a function of unit volume (E-V curves) for various hafnia phases (a) calculated from DFT at the level of PBE and (b) that calculated from the COMB potential for Hf/HfO_2 developed in this work.

both cases their energies are sufficiently higher than the monoclinic phase. For a monoclinic phase to transform to rutile/α-PbO_2-type structures, negative pressure must be applied (which corresponds to a volume expansion), accompanied by a decrease in the coordination number from 7 to 6 on all Hf atoms and 3/4 to 3 on all O atoms. The monoclinic-to-rutile/α-PbO_2 transition was never observed in considered test cases, as discussed later in this section.

The finite-temperature properties are also of significant interest. Table V gives the thermal expansion coefficients of the monoclinic phase hafnia calculated with the COMB potential, compared with those from experiments.[36] The coefficients of thermal expansion in the a and c axes are slightly overestimated relative to the experimental values while that in the b axis is in fairly good agreement. As a result, the predicted volumetric thermal-expansion coefficient is ~30% larger than experimental values.

TABLE V. Axial and volume thermal-expansion coefficients of the monoclinic hafnia calculated with the COMB potential developed in this work compared with those from experiments.

	a	b	c	V
Expt.[a]	6.1–8.4	1.2–2.7	9.6–12.6	20.6–23.5
COMB	10.52	2.11	13.89	29.46

[a]Reference 36.

We also tested the temperature dependence of the lattice parameters and axial angles of the monoclinic hafnia on heating and cooling using the COMB potential for Hf/HfO_2 developed in this work. The monoclinic phase was heated from 300 K up to 3500 K within 0.1 ns with three-dimensional periodic boundary conditions applied, the lattice parameters gradually increase due to thermal expansion and the axial angles remain fairly constant. No sign of a phase transformation was seen while the monoclinic phase melted at around 3600 K. The lattice parameters and axial angles obtained from cooling the structure that was equilibrated at 3500 K follow the heating curves back down to 300 K. Since this system does not have any nucleation site for heterogeneous nucleation, this is not compelling evidence for the absence of a structural phase transition.

To provide such a heterogeneous nucleation site, surfaces were created on the monoclinic phase by lifting the periodic boundary condition on the (100) direction. This system, in which the surfaces act a nucleation sites, transforms to the tetragonal phase upon heating after 2.2 ps at 2300 K. On undergoing the phase transition, the sevenfold Hf atoms become fully eightfold coordinated, while the threefold O atoms become fourfold coordinated. This is characteristic of a transition from the monoclinic phase to a fluorite-like phase. This transition is quantified by the change in time-averaged lattice parameters in a, b, and c axes upon heating from 2000 to 3000 K as shown in Fig. 2. It is seen that at 2300 K (around 8 ps) the a-axis spacing decreased from 5.236 to 5.196 Å while the b axis also decreased from 5.242 to 5.181 Å, which corresponds to the lattice parameter of the tetragonal phase in the a, b axes, indicating the phase transition (the measuring of a axis spacing takes the centermost

TABLE IV. Cohesive energy of monoclinic hafnia (in units of eV/HfO_2 unit) and that relative to monoclinic hafnia for six other polymorphs calculated from DFT-PBE and COMB potential for Hf/HfO_2 developed in this work.

(eV/HfO_2)	Monoclinic	α-PbO2	O1	Rutile	Tetragonal	Cubic	O2
DFT[a]	−30.45		+0.065		+0.156	+0.237	+0.385
DFT-PBE (This work)	−30.56	+0.058	+0.070	+0.109	+0.159	+0.238	+0.386
COMB	−30.69	+0.076	+0.085	+0.067	+0.178	+0.293	+0.430

[a]Reference 40.

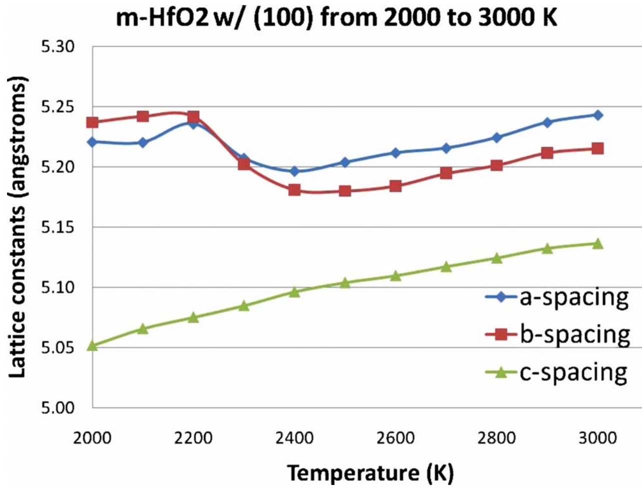

FIG. 2. (Color online) Temperature dependence of the lattice constants of monoclinic hafnia with (100) surface on heating from 2000 to 3000 K showing the monoclinic-to-tetragonal phase transition at 2300 K using the COMB potential for Hf/HfO_2 developed in this work.

two unit cells to exclude the surface effect). This phase transition is confirmed by coordination number change and radial distribution function. No further phase transition was found upon further heating. A similar surface/interface-enhanced tetragonal-to-monoclinic phase transition phenomenon has been shown in a first-principles study by Christensen and Carter[46] of the α-$Al_2O_3(1\bar{1}02)$/t-ZrO_2 (001) interface.

III. DEFECT-FORMATION ENERGIES IN MONOCLINIC HAFNIUM OXIDE

Table VI compares the formation energies for the cation and anion vacancies, interstitials and Frenkel pairs and the Schottky defects in the monoclinic phase of HfO_2 determined from the COMB potential with DFT results.[47] The defect-formation energies ΔE^f were calculated with the equation $\Delta E^f = E^{def} - E^{perf} \pm \Sigma_i n_i \mu_i$, where is E^{def} and E^{perf} are the energies of defective and perfect bulk structures, respectively, n_i is the number of defects and μ_i is the chemical potential of the defect. The chemical potential of a hafnium atom in both the metallic and oxide phases at 300 K was used in the equation to estimate hafnium-containing defects, and that of O_2 molecule at the same temperature was used for defects that contain oxygen. The charge neutrality of the system is maintained after creating the defects. For example, if we consider a Hf vacancy, a Hf ion, instead of a Hf atom, is deleted from the structure it leaves its charges (+3.48e) in the system. In contrast, when we create a Hf interstitial, a neutral Hf atom is added to the system. A cation Frenkel defect is created by introducing both a Hf ion vacancy and a Hf ion interstitial. Due to the dynamic charge-transfer feature inherent to the COMB potential, created defects are able to take on charges from the surrounding ions while maintaining charge neutrality over the system as a whole. Charges associated with interstitial defects after charge equilibration are given in parenthesis in Table VI. Two values are given for oxygen interstitials, indicating the incorporation of oxygen interstitials into threefold- or fourfold-coordinated oxygen sites, respectively. Obtaining a good estimate of defect-formation energies of the oxygen defects is particularly important since they act as charge traps and diffuse in the oxide as interstitials. Since the defect-formation energies were not part of the fitting set of physical properties, the fact that the COMB potential predicts the defect-formation energies with fidelity similar to that of DFT can be viewed as an indication that much of the correct physics is being captured.

Removing a hafnium atom from the bulk monoclinic phase results in the breaking of seven Hf-O bonds; thus the energy required to form this point defect is the greatest among Hf/O vacancies and interstitials. Similarly, creating an oxygen vacancy requires breaking three to four Hf-O bonds; hence the formation energy is less than that of the hafnium vacancy. Hf and O interstitials require less energy to form since increasing the coordination number is more energetically favorable than breaking several Hf-O bonds. Of all

TABLE VI. Defect-formation energies (in units of electron volt) of the monoclinic HfO_2 phase predicted with the COMB potential developed in this work compared with those from DFT calculations. The chemical potential of Hf in both metal and oxide phases were used to estimate the formation energies of Hf vacancy, interstitial and Schottky defect. Values in parenthesis are the charges associated with interstitial defects from DFT and COMB potential after charge equilibration, respectively.

	DFT[a]		COMB	
Defect	μ_{metal}	μ_{oxide}	μ_{metal}	μ_{oxide}
Hf vacancy	16.9	5.7	23.53	6.49
Hf interstitial			9.78 (+1.983e)	26.81 (+1.983e)
O vacancy	9.34	9.36	11.95	13.44
O interstitial	4.2	5.8 (0.0e)	3.97	5.24 (−0.002e)
Schottky			47.10	30.07
Cation Frenkel			43.29 (+1.991e)	
Anion Frenkel			18.06 (+0.101e)	

[a]Reference 47.

the point defects, the oxygen interstitial has the smallest formation energy. Also shown are the estimated defect-formation energies of Schottky defects, and cation and anion Frenkel pairs. It can be seen from Table VI that the energy required to create a Schottky defect is slightly larger than that of one Hf and two O vacancies added together. Likewise, the formation energy of the cation Frenkel pair is little larger than the sum of one Hf vacancy and one Hf interstitial defect, which indicates that the association energy of the Hf vacancy and interstitial defects are positive; this implies that these defects like to be far apart and additional energy is required to bring them close to each other. In contrast, the formation energy of the anion Frenkel is slightly smaller than the sum of constituent point defects, indicating slightly negative association energy.

IV. HAFNIUM OXIDE AND SILICON INTERFACE

Although hafnia is an excellent material for the gate oxide dielectric, problems still exist; in particular, the diffusion of oxygen through the hafnia layer to form a silica layer at the HfO_2/Si interface.[48,49] The formation of this interfacial layer between hafnia and silicon substrates, which decreases the dielectric constant and leads to material deterioration, must be suppressed. In this section, we demonstrate the ability of the COMB potential to model the HfO_2/Si interface and oxygen transport at the interface. To carry out this study, the Hf/HfO_2 potential is implemented together with the COMB potential for Si/SiO_2.[19] This is possible because the functional form and the oxygen parameters are exactly the same between the two potentials, thus allowing the oxygen to interact with both elements in a well-defined manner within the system. The short-range interaction between Hf and Si follows the Lorentz-Berthelot mixing rule described in Eqs. (A10)–(A13), and the Hf and Si ions also interact via long-range Coulombic interactions.

There are various techniques for depositing hafnia films including atomic layer deposition (ALD),[50] PLD,[51] and chemical-vapor deposition.[52] Deposited hafnia thin films are typically amorphous as deposited and polycrystalline after a postdeposition annealing.[44] It has been reported that hafnia films deposited at 300 °C by ALD are predominantly monoclinic with $(\bar{1}11)$ texture.[53,54] For this proof-of-principle demonstration of the potential developed in this work, an oxygen-terminated cubic HfO_2 (100)/Si (100) interface was chosen.

Figure 3 shows snapshots of the c-HfO_2:O/Si interface at (a) its initial condition (since the lattice parameters of c-HfO_2 and Si are fairly close, the interface is fully coherent with −8.1% strain applied to the Si substrate in the x and y directions), and (b) after 2 ps of evolution at 300 K. Large (red) atoms are Hf, medium-sized atoms (cyan) are Si, and small atoms (blue) are oxygen. The snapshots are color coded (online) according to the charges the atoms carry: red is positive, cyan is neutral, and blue is negative. Initially the c-HfO_2 layer carried $+3.30e$ on the Hf atoms and $-1.485e$ on the O atoms. The Si substrate is neutral and the system as a whole is charge neutral.

It can be seen that the interfacial Si and O atoms from the Si substrate and c-HfO_2:O, respectively, move slightly into the interface, forming Si-O bonds. As a result a very thin SiO_2 layer with oxidized Si atoms is formed. The driving mechanism for the formation of the SiO_2 layer may be a result of the unfavorable coordination of Si atoms at the interface, which are sixfold coordinated and have relatively high energy. Once the small displacement between the interfacial Si and O atoms takes place to form the SiO_2 layer, the interfacial Si atoms are fourfold coordinated, the second layer Si atoms are threefold coordinated, the interfacial Hf atoms are sixfold coordinated, and the oxygen atoms are threefold or fourfold coordinated. This results in a more stable bonding environment at the interface than the starting structure.

Figure 4 illustrates the distribution of charge at the c-HfO_2/Si interface for Si, O, and Hf atoms after 2 ps of evolution. At the interface, the change in charge on Si atoms is $+2.308e$ on average, while that for O and Hf atoms are $-0.413e$ and $+0.383e$, respectively. The results indicate that interfacial Si atoms oxidize, forming Si-O bonds and donating electrons to the O atoms in the cubic hafnia. The oxidation of Si atoms at the interface to form a silica layer is consistent with experimental results;[48,49] as we shall see, these strong Si-O bonds contribute to the large value of the work of adhesion.

The work of adhesion quantifies the energy saving from two surfaces forming an interface, and is an indication of the stability and strength of the interface. The larger the work of adhesion of an interface, the more energy is required to separate the interface into two surfaces. Here the work of adhesion W of the c-HfO_2/Si interface was calculated from the standard equation: $W=(E_{HfO_2}+E_{Si}-E_{HfO_2/Si})/A$, where E_{HfO_2} and E_{Si} are the total potential energy of the relaxed fixed-volume HfO_2 and Si slabs, respectively, $E_{HfO_2/Si}$ is the energy of the relaxed interfacial structure, and A is the surface/interface area. The same method was applied to calculate the work of adhesion of Cu/SiO_2 interfaces with DFT.[55] All the structures are equilibrated at 300 K, prior to quenching at $T=0$ K. The calculated work of adhesion of the quenched c-HfO_2/Si is 7.36 J/m^2, which indicates a relatively strong interface, and is in excellent agreement with that calculated from DFT-PBE, 7.19 J/m^2. The surface energies calculated from the relaxed c-HfO_2 (100) and Si (100) slabs with COMB potential are 5.74 J/m^2 and 3.03 J/m^2, respectively, compared to those obtained from DFT calculations, which are 5.56 J/m^2 and 2.83 J/m^2, respectively. Note that the Si (100) surface energy is high because of the −8.1% strain applied to (010) and (001) directions.

The agreement between the COMB prediction and the DFT calculation indicates that the COMB potentials for Hf/HfO_2 and Si/SiO_2 in combination with the mixing rule for Hf/Si interactions is adequate for modeling Si/HfO_2 interfaces. However, additional extensive testing is required to identify cases for which this approach works less well. It should be mentioned that Si (100) and monoclinic hafnia (001) and $(\bar{1}11)$ interfaces are currently being constructed and tested, and the results are reserved for a future study.

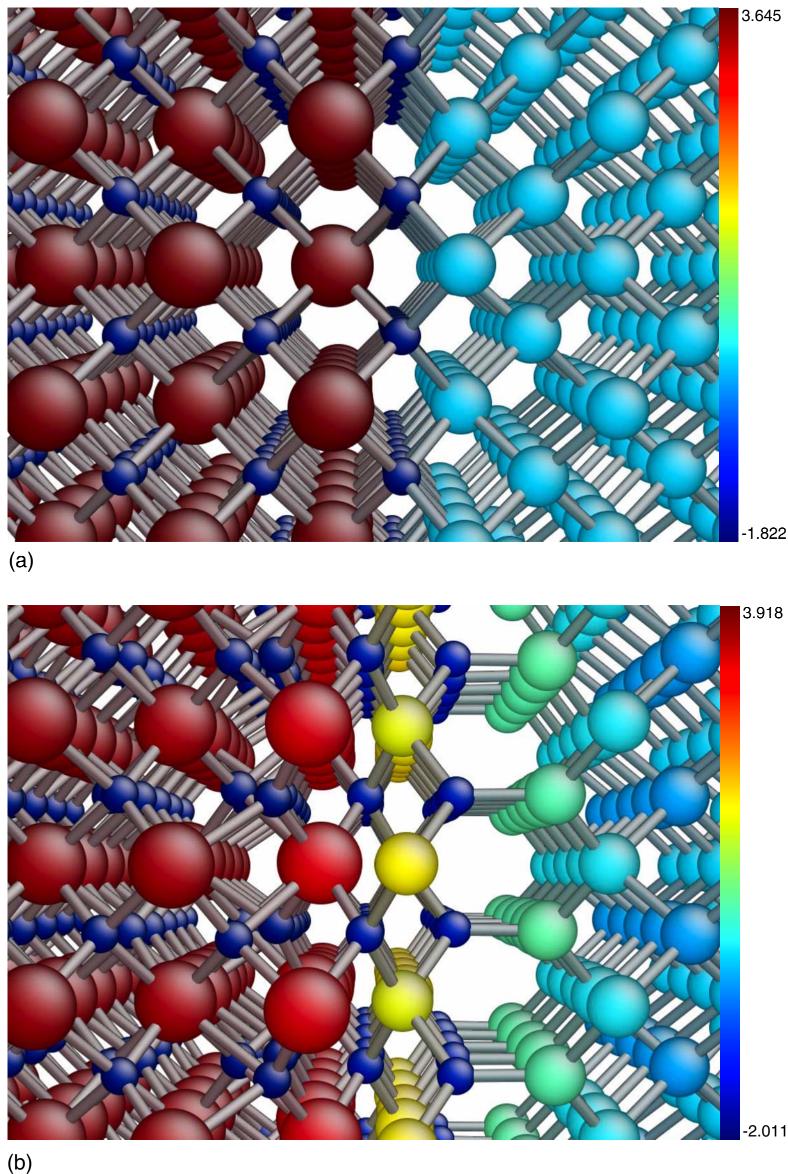

FIG. 3. (Color online) Snapshots of the cubic HfO_2 and Si (c-HfO_2/Si) interfacial structure evolving at 300K (a) 0 ps, (b) 2.0 ps. Large (red) atoms are Hf, medium sized atoms (cyan) are Si and small atoms (blue) are oxygen.

V. CONCLUSIONS

The COMB potential for Hf/HfO_2 developed in this work is based on the Tersoff potential for silicon,[21,22] which incorporates many-body effects that allow the breaking of existing bonds and the formation of new bonds; the Yasukawa[23] modification of the Tersoff potential for Si/SiO_2 that introduces dynamic charge transfer; and the COMB potential for Cu/Cu_2O (Ref. 20) that incorporates direct sum of modules for treating long-range electrostatic interactions. The COMB potential for Hf/HfO_2 captures most of the physical properties of Hf metal and hafnia polymorphs. However, it is necessary to sacrifice accuracy in some properties, such as the Hf metal lattice constants and cohesive energy, in order to guarantee the correct phase order among hafnia polymorphs. Most importantly, however, the COMB potentials for Hf/HfO_2, Cu/Cu_2O (Ref. 20) and Si/SiO_2 (Ref. 19) can be seamlessly coupled together for MD simulation studies of life-size devices such as HfO_2/Si interfaces, $Hf_xSi_{1-x}O_y$ films, the growth of hafnia films on Si or SiO_2, and the entire gate stack (Si/SiO_2/HfO_2/Cu_2O/Cu). Thus, the COMB potential for Hf/HfO_2 should prove to be a useful tool and an effective method for carrying out large-scale MD simulations and computational studies.

ACKNOWLEDGMENTS

We gratefully acknowledge the financial support of the National Science Foundation under Grant No. DMR-0426870 and a grant of computer time from the High Performance Computing Center at the University of Florida.

APPENDIX: FUNCTIONAL FORM OF THE COMB POTENTIAL FOR Hf/HfO_2

The COMB potential for Hf/HfO_2 has the general functional form,

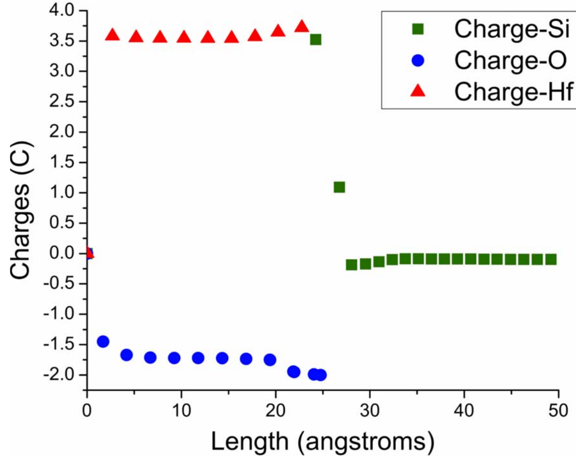

FIG. 4. (Color online) Charge distribution of the c-HfO$_2$/Si interface for Si (square symbols), O (circle symbols) and Hf (triangle symbols) atoms after 2 ps evolution.

$$E_T = \sum_i \left[E_i^S + \frac{1}{2} \sum_{j \neq i} V_{ij}(r_{ij}, q_i, q_j) + E_i^{BB} \right], \quad \text{(A1)}$$

where E_T is the total potential energy of the system, E_i^S is the self-energy term of atom i, V_{ij} is the interatomic potential between the ith and jth atoms, r_{ij} is the distance of the atoms i and j, and q_i and q_j are charges of the atoms, and E_i^{BB} is the bond-bending term of atom i. The interatomic potential energy V_{ij} consists of four components: short-range repulsion, U_{ij}^R, short-range attraction, U_{ij}^A, long-range Coulombic interaction, U_{ij}^I, and long-range van der Waals energy, U_{ij}^V, which are defined as,

$$V_{ij}(r_{ij}, q_i, q_j) = U_{ij}^R(r_{ij}) + U_{ij}^A(r_{ij}, q_i, q_j) + U_{ij}^I(r_{ij}, q_i, q_j) + U_{ij}^V(r_{ij}), \quad \text{(A2)}$$

$$U_{ij}^R(r_{ij}) = f_{S_{ij}} A_{ij} e^{(-\lambda_{ij} r_{ij})}, \quad \text{(A3)}$$

$$U_{ij}^A(r_{ij}, q_i, q_j) = -f_{S_{ij}} b_{ij} B_{ij} e^{(-\alpha_{ij} r_{ij})}, \quad \text{(A4)}$$

$$U_{ij}^I(r_{ij}, q_i, q_j) = J_{ij}(r_{ij}) q_i q_j, \quad \text{(A5)}$$

$$U_{ij}^V(r_{ij}) = f_{L_{ij}} (C_{VDW_i} C_{VDWj})^{1/2} / r_{ij}^6. \quad \text{(A6)}$$

The many-body effects are described with the bond-order term, b_{ij}, in the short-range attraction, and it has the form

$$b_{ij} = \left\{ 1 + \left[\beta_i \sum_{k \neq i,j} \xi_{ijk} g(\theta_{jik}) \right]^{n_i} \right\}^{-1/(2n_i)}, \quad \text{(A7)}$$

where the symmetry function ζ_{ijk} and angular function $g(\theta_{jik})$ are defined as

$$\zeta_{ijk} = f_{S_{ik}} e^{[\alpha_{ij}^{m_i} (r_{ij} - r_{ik})^{m_i}]}, \quad \text{(A8)}$$

$$g(\theta_{jik}) = 1 + c_i^2/d_i^2 - c_i^2/[d_i^2 + (h_i - \cos\, \theta_{jik})^2]. \quad \text{(A9)}$$

Here θ_{jik} is the bond angle between bonds ij and ik. The inverse decay lengths λ_{ij} and α_{ij}, the leading coefficients A_{ij} and B_{ij} depend only on the types of interacting atoms and follow the venerable Lorentz-Berthelot[56] mixing rules,

$$\lambda_{ij} = (\lambda_i + \lambda_j)/2, \quad \text{(A10)}$$

$$\alpha_{ij} = (\alpha_i + \alpha_j)/2, \quad \text{(A11)}$$

$$A_{ij} = \sqrt{A_{S_i} A_{S_j}}, \quad \text{(A12)}$$

$$B_{ij} = \sqrt{B_{S_i} B_{S_j}}, \quad \text{(A13)}$$

where A_{S_i} and B_{S_i} depend on the charge of the atom i,

$$A_{S_i} = A_i e^{(\lambda_i D_i)}, \quad \text{(A14)}$$

$$B_{S_i} = B_i e^{(\alpha_i D_i)} [a_{B_i} - |b_{B_i}(q_i - Q_{O_i})|^{n_{B_i}}], \quad \text{(A15)}$$

$$D_i = D_{U_i} + |b_{D_i}(Q_{U_i} - q_i)|^{n_{D_i}}, \quad \text{(A16)}$$

$$b_{D_i} = (D_{L_i} - D_{U_i})^{1/n_{D_i}} / (Q_{U_i} - Q_{L_i}), \quad \text{(A17)}$$

$$n_{D_i} = \ln[D_{U_i}/(D_{U_i} - D_{L_i})] / \ln[Q_{U_i}/(Q_{U_i} - Q_{L_i})], \quad \text{(A18)}$$

$$b_{B_i} = |a_{B_i}|^{1/n_{B_i}} / \Delta Q_i, \quad \text{(A19)}$$

$$a_{B_i} = 1/(1 - |Q_{O_i}/\Delta Q_i|^{n_{B_i}}), \quad \text{(A20)}$$

$$\Delta Q_i = (Q_{U_i} - Q_{L_i})/2, \quad \text{(A21)}$$

$$Q_{O_i} = (Q_{U_i} + Q_{L_i})/2. \quad \text{(A22)}$$

The potential is truncated by the cutoff function $f_{S_{ij}}$, which is defined as,

$$f_{S_{ij}} = f_c[r_{ij}, (R_{S_i} R_{S_j})^{1/2}, (S_{S_i} S_{S_j})^{1/2}], \quad \text{(A23)}$$

$$f_c(r, R, S) = \begin{cases} 1 & r \leq R \\ \{1/2 + (1/2)\cos[\pi(r-R)/(S-R)]\} & R < r < S \\ 0 & r \geq S, \end{cases} \quad \text{(A24)}$$

where R and S are optimized cutoff radii.

The long-range Coulombic interaction between charged atoms is described with the charge coupling factor, $J_{ij}(r_{ij})$, and takes the form,

$$J_{ij}(r_{ij}) = \int d^3 r_i \int d^3 r_j \rho_i(r_i,q_i)\rho_j(r_j,q_j)/r_{ij}, \quad \text{(A25)}$$

$$\rho_i(r_i,q_i) = q_i \frac{\xi_i^3}{\pi} e^{(-2\xi_i|r_{ij}-r_i|)}, \quad \text{(A26)}$$

which is a Coulomb integral over 1s-type Slater orbitals, where ξ_i is an orbital exponent that controls the radial decay of the density. A penalty function that captures the change in self-energy due to the field of the ionic lattice is added to the self-energy term $E_i^S(q_i)$ and takes the form,

$$V_i^S(r,q_j) = \frac{1}{4\pi\varepsilon_o} \sum_{j\neq i}^{NN} \left(\frac{\rho_1 q_j^2}{r_{ij}^5} - \frac{\rho_2 q_j}{r_{ij}^5} \right). \quad \text{(A27)}$$

The self-energy term E_i^S describes the energy required to form a charge and takes the form,

$$E_i^S(q_i) = \chi_i q_i + J_i q_i^2 + K_i q_i^3 + L_i q_i^4, \quad \text{(A28)}$$

where the coefficients χ_i, J_i, K_i, and L_i are fit to the atomic hafnium and oxygen ionization energies and electron affinities. The oxygen coefficients are the same as the COMB potentials for Si/SiO_2 for amorphous silica[19] to ensure full compatibility and transferability of the different potentials.

The bond-bending term E_i^{BB}, applied to Hf-Hf-Hf bonds, is defined as,

$$E_{\text{Hf-Hf-Hf}} = \sum_i \sum_{j\neq i} \sum_{k\neq i,j} f_{S_{ij}} f_{S_{ik}} [K_{LP} P^6(\cos\theta_{\text{Hf-Hf-Hf}})], \quad \text{(A29)}$$

where P^6 is the third-order Legendre polynomial function of the Hf-Hf-Hf bond angle and K_{LP}^6 is the coefficient fitted to the difference in cohesive energies of Hf in hcp and fcc phases.

*Corresponding author; sphil@mse.ufl.edu

[1] G. M. Rignanese, J. Phys.: Condens. Matter **17**, R357 (2005).
[2] X. Y. Zhao and D. Vanderbilt, Phys. Rev. B **65**, 233106 (2002).
[3] E. P. Gusev, C. Cabral, M. Copel, C. D'Emic, and M. Gribelyuk, Microelectron. Eng. **69**, 145 (2003).
[4] H. Watanabe, S. Kamiyama, N. Umezawa, K. Shiraishi, S. Yoshida, Y. Watanabe, T. Arikado, T. Chikyow, K. Yamada, and K. Yasutake, Jpn. J. Appl. Phys., Part 2 **44**, L1333 (2005).
[5] N. Umezawa, K. Shiraishi, T. Ohno, H. Watanabe, T. Chikyow, K. Torii, K. Yamabe, K. Yamada, H. Kitajima, and T. Arikado, Appl. Phys. Lett. **86**, 143507 (2005).
[6] V. Cuny and N. Richard, J. Appl. Phys. **104**, 033709 (2008).
[7] K. Tse and J. Robertson, Appl. Phys. Lett. **89**, 142914 (2006).
[8] K. Xiong and J. Robertson, Microelectron. Eng. **80**, 408 (2005).
[9] P. F. Lee, J. Y. Dai, K. H. Wong, H. L. W. Chan, and C. L. Choy, J. Appl. Phys. **93**, 3665 (2003).
[10] R. Choi, S. C. Song, C. D. Young, G. Bersuker, and B. H. Lee, Appl. Phys. Lett. **87**, 122901 (2005).
[11] R. M. Nieminen, M. H. Hakala, and A. S. Foster, Mater. Sci. Semicond. Process. **9**, 928 (2006).
[12] R. C. Weast, *Handbook of Chemistry and Physics* (Chemical Rubber, Cleveland, Ohio, 1969).
[13] J. M. Leger, A. Atouf, P. E. Tomaszewski, and A. S. Pereira, Phys. Rev. B **48**, 93 (1993).
[14] M. Balog, M. Schieber, M. Michman, and S. Patai, Thin Solid Films **41**, 247 (1977).
[15] R. McWeeny, *Methods of Molecular Quantum Mechanics* (Academic, New York, 1989).
[16] P. Hohenberg and W. Kohn, Phys. Rev. **136**, B864 (1964).
[17] W. Kohn and L. J. Sham, Phys. Rev. **140**, A1133 (1965).
[18] J. G. Yu, S. B. Sinnott, and S. R. Phillpot, Phys. Rev. B **75**, 085311 (2007).
[19] T.-R. Shan, B. D. Devine, J. W. Hawkins, A. A. Asthagiri, S. R. Phillpot, and S. B. Sinnott (unpublished).
[20] B. D. Devine, T.-R. Shan, S. B. Sinnott, and S. R. Phillpot (unpublished).
[21] J. Tersoff, Phys. Rev. B **37**, 6991 (1988).
[22] J. Tersoff, Phys. Rev. B **38**, 9902 (1988).
[23] A. Yasukawa, JSME Int. J., Ser. A **39**, 313 (1996).
[24] A. K. Rappe and W. A. Goddard, J. Phys. Chem. **95**, 3358 (1991).
[25] F. H. Streitz and J. W. Mintmire, Phys. Rev. B **50**, 11996 (1994).
[26] T. Iwasaki, J. Mater. Res. **19**, 1197 (2004).
[27] T. Iwasaki, J. Mater. Res. **20**, 1300 (2005).
[28] J. C. Slater, Phys. Rev. **36**, 57 (1930).
[29] I. T. Adamson, *Elementary Rings and Modules* (University Mathematical Texts, Oliver and Boyd, Edinburgh, 1972).
[30] B. J. Thijsse, Nucl. Instrum. Methods Phys. Res. B **228**, 198 (2005).
[31] J. Yu, S. B. Sinnott, and S. R. Phillpot, Philos. Mag. Lett. **89**, 136 (2009).
[32] A. C. T. van Duin, S. Dasgupta, F. Lorant, and W. A. Goddard, J. Phys. Chem. A **105**, 9396 (2001).
[33] P. K. Schelling, S. R. Phillpot, and D. Wolf, J. Am. Ceram. Soc. **84**, 1609 (2001).
[34] M. Wilson, U. Schonberger, and M. W. Finnis, Phys. Rev. B **54**, 9147 (1996).
[35] S. Fabris, A. T. Paxton, and M. W. Finnis, Phys. Rev. B **61**, 6617 (2000).
[36] J. Wang, H. P. Li, and R. Stevens, J. Mater. Sci. **27**, 5397 (1992).
[37] D. M. Adams, S. Leonard, D. R. Russell, and R. J. Cernik, J. Phys. Chem. Solids **52**, 1181 (1991).
[38] D. W. Stacy, J. K. Johnstone, and D. R. Wilder, J. Am. Ceram. Soc. **55**, 482 (1972).
[39] C. K. Lee, E. N. Cho, H. S. Lee, C. S. Hwang, and S. W. Han, Phys. Rev. B **78**, 012102 (2008).

[40] J. E. Jaffe, R. A. Bachorz, and M. Gutowski, Phys. Rev. B **72**, 144107 (2005).
[41] J. E. Lowther, J. K. Dewhurst, J. M. Leger, and J. Haines, Phys. Rev. B **60**, 14485 (1999).
[42] S. Desgreniers and K. Lagarec, Phys. Rev. B **59**, 8467 (1999).
[43] C. A. Ponce, R. A. Casali, and M. A. Caravaca, J. Phys.: Condens. Matter **20**, 045213 (2008).
[44] X. Luo, A. A. Demkov, D. Triyoso, P. Fejes, R. Gregory, and S. Zollner, Phys. Rev. B **78**, 245314 (2008).
[45] J. P. Perdew, K. Burke, and M. Ernzerhof, Phys. Rev. Lett. **77**, 3865 (1996).
[46] A. Christensen and E. A. Carter, Phys. Rev. B **62**, 16968 (2000).
[47] A. S. Foster, F. L. Gejo, A. L. Shluger, and R. M. Nieminen, Phys. Rev. B **65**, 174117 (2002).
[48] H. Wong and H. Iwai, Microelectron. Eng. **83**, 1867 (2006).
[49] K. Cherkaoui, S. Monaghan, M. A. Negara, M. Modreanu, P. K. Hurley, D. O'Connell, S. McDonnell, G. Hughes, S. Wright, R. C. Barklie, P. Bailey, and T. C. Q. Noakes, J. Appl. Phys. **104**, 064113 (2008).
[50] M. Ritala, M. Leskela, L. Niinisto, T. Prohaska, G. Friedbacher, and M. Grasserbauer, Thin Solid Films **250**, 72 (1994).
[51] S. V. Ushakov, A. Navrotsky, Y. Yang, S. Stemmer, K. Kukli, M. Ritala, M. A. Leskelä, P. Fejes, A. Demkov, C. Wang, B.-Y. Nguyen, D. Triyoso, and P. Tobin, Phys. Status Solidi B **241**, 2268 (2004).
[52] Q. Fang, J. Y. Zhang, Z. Wang, M. Modreanu, B. J. O'Sullivan, P. K. Hurley, T. L. Leedham, D. Hywel, M. A. Audier, C. Jimenez, J.-P. Senateur, and I. W. Boyd, Thin Solid Films **453-454**, 203 (2004).
[53] M. Y. Ho, H. Gong, G. D. Wilk, B. W. Busch, M. L. Green, P. M. Voyles, D. A. Muller, M. Bude, W. H. Lin, A. See, M. E. Loomans, S. K. Lahin, and P. I. Räisänen, J. Appl. Phys. **93**, 1477 (2003).
[54] D. Triyoso, R. Liu, D. Roan, M. Ramon, N. V. Edwards, R. Gregory, D. Werho, J. Kulik, G. Tam, E. Irwin, X.-D. Wang, L. B. La, C. Hobbs, R. Garcia, J. Baker, B. E. White, Jr., and P. Tobina, J. Electrochem. Soc. **151**, F220 (2004).
[55] K. Nagao, J. B. Neaton, and N. W. Ashcroft, Phys. Rev. B **68**, 125403 (2003).
[56] M. P. Allen and D. J. Tildesley, *Computer Simulation of Liquids* (Oxford University Press, New York, 1989).